Incorporation of phase change materials in fire protective clothing considering the presence of water

André Fonseca Malaquias [a,b,*], S.F. Neves [a,b], J.B.L.M. Campos [a,b]

[a] *CEFT - Transport Phenomena Research Center, Faculty of Engineering, University of Porto, Rua Dr. Roberto Frias, 4200-465 Porto, Portugal*
[b] *ALiCE - Associate Laboratory in Chemical Engineering, Faculty of Engineering, University of Porto, Rua Dr. Roberto Frias, 4200-465 Porto, Portugal*

ARTICLE INFO

ABSTRACT

When firefighters face a heat exposure, free water may be present in the fire protective clothing (FPC). Recently, the incorporation of Phase Change Materials (PCMs) into FPC has shown great promise to increase thermal performance when in the dry state. However, the presence of water in firefighting garments is expected and how this alters the thermal behavior of a PCM FPC assembly still remains to be discussed in the literature. Hence, this study concerns the effect of free water presence in the outer shell and/or thermal inner of a PCM FPC assembly consisting of 3 layers. A new mathematical model is proposed where the PCM is assumed to be incorporated in the thermal inner. A numerical analysis is performed where PCM textile latent heat, water distribution, and heat flux intensity are varied. Skin temperature, skin heat flux, and PCM liquid fraction profiles are obtained along with second-degree burn times to measure thermal performance. It is found that steam condensation at the skin reduces PCM liquid fraction at second-degree burn time, when compared to the dry case. This study tends to shine a light on the importance of considering moisture management in PCM FPC assemblies so as to promote maximum PCM efficiency.

1. Introduction

The presence of moisture in textiles tends to have a major influence on their thermal performance. When donned, the accumulation of water in textiles may originate from the surrounding environment, or from the user itself . During deployments, firefighters may sweat profusely and be exposed to external water sources such as humid environments and hose spraying. The development of improved firefighter garments demands the most increased understanding of the interdependency of the thermal performance of fire protective clothing with the contained water.

In the literature, there are several studies concerning the heat and moisture transport in a typical fire protective clothing (FPC) assembly. Barker et al. [1] experimentally studied the effect of free water presence in thermal inners when the FPC is subject to a low-heat flux exposure. The authors utilized a quartz tube heat source along with a calorimeter to measure the incoming heat flux from the turnout gear. Su et al. [2] used an improved benchtop tester to determine firefighter second–degree burn times, when exposed to a radiative heat flux and hot steam. The authors utilized a black–ceramic heat source to produce a low–heat flux exposure and a water-cooled Schmidt-Boetler thermopile type

sensor to register the incoming heat flux from the turnout suit. Keiser et al. [3] analyzed moisture distributions in FPC assemblies using a sweating torso equipment that mimicked firefighter continuous sweating. FPC layers were weighed before and after each trial to account for the accumulation of water in each of the garment layers. The same sweating torso equipment was utilized in a later study where a radiative heat source was added to the experimental setup, and the interaction between continuous sweating and radiative heat exposure on the FPC assembly was analyzed [4]. Keiser et al. [5] measured the temperatures between the layers of an FPC assembly sample initially wet and exposed to an infrared lamp heat source in a PEEK tube. The temperature profiles obtained were used as indirect evidence for moisture transport in the FPC assembly, which, in a subsequent study, was confirmed utilizing X-ray radiography to analyze the position and quantity of water in the FPC assembly [6]. Mandal et al. [7] proposed a new protocol to characterize the thermal protective performance of fabrics in hot water exposure where heat and mass transfer through the FPC assembly is emphasized.

Several numerical studies also exist in the literature regarding heat and mass transport in FPCs. Chitrphiromsri et al. [8] adapted Gibson's

---

Fig. 1. PCM FPC - skin system used in numerical simulations.

model [9] to numerically study heat and mass transport in a wet FPC assembly under high-intensity heat exposure. Huang et al. [10] also proposed a heat and mass transfer model for FPCs which considers air gaps between the textile layers. Su et al. [11] developed and validated a heat and mass transfer model for FPCs subject to hot steam exposure. The authors report on the importance of mass transfer under such conditions as the hot steam diffuses rapidly through the turnout and condenses near the sensor. Su et al. [12] then suggested and validated a heat and mass transfer model for FPCs under low dry heat exposures where the initial presence of moisture in the FPC was considered.

Efforts to improve thermal performance of FPC are vast, and researchers are constantly trying to find new ways to enhance their thermal comfort capabilities and heat resistance [13–16]. One of the solutions that is being looked upon with promise is the incorporation of phase change materials in firefighting garments. A phase change material (PCM) is a substance in which the latent heat associated with its phase change (usually solid-liquid) can be used to improve thermal management. In the case of incorporation into a FPC, the PCM would have the role of absorbing part of the incoming heat flux from the flame as latent energy, thus hindering temperature rise in the FPC and, consequently, at the firefighters' skin. Several studies exist in the literature reporting on the potential benefits of PCM incorporation in a FPC [17–22].

In the literature, it is not common to find PCMs in textile applications where the effect of heat and moisture is simultaneously studied. Fengzhi et al. [23] proposed a heat and mass transport mathematical model for textiles with incorporated micro-PCMs. The model was validated for an ambient step temperature variation. Itan et al. [24] studied the thermal effect provided by the incorporation of PCM – desiccant packets onto a cooling vest that was subject to a hot humid environment. A mathematical model was proposed and validated. A decrease in the humidity content at the microclimate and an increase in the amount of liquefied PCM were observed, due to the desiccant layer. Wan et al. [25] proposed a heat and moisture transfer model for hybrid personal cooling garments incorporating PCMs and ventilation fans. The model was validated with experimental data, and good agreement was found. Zhao et al. [26] reported on the disadvantages of wearing PCM cooling vests in hot dry conditions, as the presence of PCM packets dramatically reduces the permeability of the fabric assembly, hindering evaporative cooling from the user.

In practice, several techniques exist to incorporate PCMs into a textile substrate [27]. The PCM can be already encapsulated in a micro or nanocapsule and then incorporated into the textile. Renzi et al. [28] incorporated microencapsulated PCMs (mPCMs) into a leather textile utilizing a wet soaking and a dry coating method. The authors found a limiting thermal effect on the jacket and reported that such depends on the percentage of incorporated PCM. Fiber latent heat of 20.4 J/g was reported for a 40 % wt. microPCM incorporation. Bendkowska et al. [29] applied mPCMs to non-woven textiles and noticed a thermoregulating effect. The authors note that the extension of such effect depends on the amount of incorporated PCM, its distribution, and position in the textile. Yoo et al. [30] incorporated 100% cotton textiles with mPCMs using the knife over roll technique and studied the thermal response of a multilayer garment system consisting of such textiles. The cotton layers were

Table 1
– Properties of the various layers consisting of the firefighting protective clothing.

Property	Outer shell	Moisture Barrier	Thermal inner	Source
Thickness (w) mm	0.39	0.45	2.24	[32]
Density (ρ_{ds}) [a]kg/m^3	1460	1460	1440	[33]
Specific heat (c_{ds}) J/(kg·K)	1086	1086	1421	[34]
Thermal conductivity (k_{ds}) W/(m·K)	0.25	0.25	0.21	[33,34]
Fiber volume fraction (ε_{ds})	0.36	0.16	0.09	Estimated [32,35]
Tortuosity (τ)	2.32	2.87	1.32	Estimated [36]
Fiber diameter (d_f) µm	15	15	15	[37,38]
Regain at 65% RH	0.0485	0.0485	0.0397	[39]
Diffusivity of water in fiber (D_f) m^2/s	6×10^{-14}	6×10^{-14}	6×10^{-14}	[8]
Proportionality constant for liquid water sorption in fibres (γ_{ls}) kg/m^3	5×10^{-4}	5×10^{-4}	5×10^{-4}	[8]

[a] Please put units in the property column below the variable name and symbol. They should also be centered with the text if possible.

incorporated with mPCMs so as to study the effect of mPCM distribution in the assembly. The authors noticed a thermal buffering effect that depends on the number of layers with incorporated mPCMs, and their position in the assembly. Rossi et al. [31] incorporated mPCMs into a foam which was then coated onto a thermal inner of a firefighting garment assembly. The PCM foam layer weighed about 180 g/m^2. The authors found that the mPCM garment has a thermal buffering effect when exposed to a heat source. Su et al. [19] coated different contents of mPCMs, with different melting temperatures, onto a thermal protective clothing garment and studied the performance of the assembly under hot contact exposure. The authors noticed a beneficial thermal effect that depends on the incorporated PCM's quantity, melting temperature, and latent heat. In the literature, several authors report on their PCM textile fibers to have latent heats in the range 1–44 J/g [27].

Currently, according to the authors' knowledge, there is no numerical study in the literature analyzing heat and moisture transport in a PCM FPC (i.e., phase change material incorporated in fire protective clothing). Unlike the lower temperature applications described above, the heat and moisture transfer in wet FPC assemblies is characterized by high temperature and vapor concentrations which can significantly influence PCM thermal behavior. In previous works, the current group studied correlations regarding the choice of a PCM to be incorporated in a dry firefighting garment [17,22], neglecting the effect of moisture on the performance of the PCM FPC. Thus in this study, the presence of free water and, consequently, moisture transport in a PCM FPC suit is considered, and their effects in the PCM selection criteria are discussed. Moreover, in this study, the PCM incorporated layer is considered permeable, rather than impermeable, to water and to water vapor (in our previous works [17,22], the layer was considered to be a PCM slab). Firstly, the effect of incorporating different PCM quantities in the

Table 2
Properties of Rubitherm® RT42 [40].

Property	Value
Latent heat (λ)	220 kJ/kg
Specific heat (C_{PCM})	2 kJ/(kg·K)
Solid density (ρ_{PCM})	800 kg/m³
Thermal conductivity (k_{PCM})	0.2 W/(m·K)
Melting temperature (T_m)	42.5 °C
Floating variable (T_0)	1 °C

thermal inner on second-degree burn time is studied, initially considering a saturated wet outer shell. Then, the effect of PCM melting temperature on second-degree burn time is analyzed for dry and wet PCM FPC assembly samples considering different initial water distributions. This is done for high – medium- and low – intensity exposures.

2. Materials and methods

2.1. Problem description

Consider a typical 3 – layered FPC assembly consisting of an outer shell, moisture barrier, and thermal inner, as shown in Fig. 1. In this work, to increase the thermal performance of the FPC assembly, a phase change material (PCM) is added to the thermal inner, creating a phase change material fire protective clothing (PCM FPC) assembly. The properties of each of the fabric layers utilized (without PCM incorporation) are shown in Table 1. The PCM properties are shown in Table 2.

The PCM FPC assembly is assumed to be in direct contact with the firefighters' skin composed of three layers: the epidermis, dermis and subcutaneous regions (Fig. 1). The outer shell, thermal inner, or both layers are assumed to be initially wet.

The PCM FPC assembly is then exposed to a given heat flux (section 2.4). In this scenario, garment temperature is expected to rise and water to evaporate. The vapor may then diffuse towards the skin, or towards the environment. The vapor which diffuses towards the skin may re-condense, where latent heat is released, and thus an increase in skin temperature is noted. Adding PCMs to a thermal inner could alter heat and moisture transport in the assembly and thus the amount of re – condensed vapor at the skin.

A mathematical model considering the interdependency between moisture and heat transfer phenomena is utilized to develop correlations for PCM adequate selection and textile latent heat necessary to prevent second-degree burns for a specific exposure time. As vapor re-condensation near the skin causes its temperature to rise (promoting skin burns), it is expected that the correlations will be influenced by the effectiveness of the PCM in preventing vapor from re - condensing near the skin.

2.2. Incorporation of PCM in the thermal inner

In practice, several techniques exist to incorporate a PCM into a textile [27]. Beyond direct incorporation, the PCM can be encapsulated in a micro or nanocapsules and then incorporated into the textile. However, whether the thermal buffering effect offered by such textiles is sufficient or not, is debatable. This doubt exists because current micro or nanocapsule incorporation techniques simply do not allow enough PCM mass to be incorporated into the textile to notice a substantial thermal buffering effect [41].

Table 3
Fiber latent heats and respective PCM volume fractions used in the simulations.

Property	Value
PCM volume fraction (ε_{PCM})	0.04–0.60
Fiber latent heat ($\lambda_{fiber,eff}$)	40–170 J/g

Thus, to link our work to current methods of incorporation of PCM, a maximum practical value of textile latent heat (i.e., 40 J/g) was set considering experimental data found in the literature [27]. Also, in this study, higher fiber latent heats are considered, representing a new incorporation method where more PCM is retained in the textile fiber, as such could be possible in the future. It is assumed that the PCMs distribution along the thermal inner textile is perfectly homogeneous and does not influence the hygroscopic properties of the textile. This implies that the PCM is incorporated in the textile pores and does not come into contact with the textile fibers. The properties of the incorporated PCM are shown in Table 2. The textile latent heats considered in the simulations are shown in Table 3.

2.3. Mathematical model and assumptions

2.3.1. Textile model

The model utilized in this work is in the sequence of a previous one, developed by our group, now including the PCM effect. The textile is considered a structure where the fiber, air pore and PCM are assumed to be homogeneous. Thus, the constitutive element of the model contemplates the presence of all phases. In this way, the model is simplified and problems with geometrical boundaries regarding the different phases are eliminated [9].

More details about the model can be found in the previous work by the group. In this section, the emphasis will be majorly put on the altered parts.

With the inclusion of a PCM phase, the energy balance in the thermal inner is stated as follows:

$$\rho_{eff} C_{eff} \frac{\partial T}{\partial t} + \frac{\partial}{\partial x}\left(-k_{eff}\frac{\partial T}{\partial x}\right) - \dot{m}_{gs}\left(\Delta h_{vap} + \Delta h_l\right) - \dot{m}_{gl}\Delta h_{vap} - \dot{m}_{ls}\Delta h_l = 0$$

(1a)

$$\rho_{eff} = \varepsilon_{bw}\rho_w + \varepsilon_\gamma \rho_\gamma + \varepsilon_{ds}\rho_{ds} + \varepsilon_{PCM}\rho_{PCM} + \varepsilon_l \rho_w$$

(1b)

$$C_{p,eff} = \frac{\varepsilon_{bw}\rho_w C_{p,w} + \varepsilon_\gamma\left(\rho_a C_{p,a} + \rho_v C_{p,v}\right) + \varepsilon_{ds}\rho_{ds}C_{p,ds} + \varepsilon_{PCM}\rho_{PCM}C_{app} + \varepsilon_l\rho_w C_{p,w}}{\rho_{eff}}$$

(1c)

$$k_{eff} = k_\gamma \left\{ \frac{\varepsilon_\gamma k_\gamma + [I + \varepsilon_{bw} + \varepsilon_{ds} + \varepsilon_{PCM} + \varepsilon_l]k_\sigma}{\varepsilon_\gamma k_\sigma + [I + \varepsilon_{bw} + \varepsilon_{ds} + \varepsilon_{PCM} + \varepsilon_l]k_\gamma} \right\}$$

(1d)

where, ρ_{eff}, C_{eff}, k_{eff}, $\dot{m}_{gs}$, $\dot{m}_{gl}$, $\dot{m}_{ls}$, Δh_{vap} and Δh_l represent the effective density, effective specific heat, effective thermal conductivity, gas sorption/desorption rate, vaporization/condensation rate, liquid sorption/desorption rate, water vaporization heat, and liquid sorption/desorption heat, respectively. ε represents the phase volume fraction, and the subscripts bw, w, γ, ds, and l stand for bounded water, water, gas, fiber, and liquid, respectively. The apparent PCM specific heat (C_{app}) is defined as follows:

$$C_{app} = \frac{dH}{dT} = \frac{d}{dT}\left[0.5 \times \lambda \times \text{erf}\left(\frac{T - T_m}{T_0}\right) + C_{PCM}(T - T_m)\right] = \lambda \times \frac{\exp\left(-\frac{T-T_m}{T_0}\right)^2}{T_0\sqrt{\pi}} + C_{PCM}$$

(1e)

where T, T_m, λ, T_0, C_{PCM} stand for the temperature, melting temperature, latent heat, floating variable associated to mushy region, and PCM specific heat, respectively.

The first term on the left-hand side of eq. (1a) accounts for the heat accumulation in the garment. The second term accounts for the conductive heat fluxes, while the third, fourth and fifth terms account for the latent heat associated with water sorption/desorption, vaporization/condensation and liquid sorption/desorption into the fibers, respectively. k_σ and k_γ represent the solid and gas phases thermal conductivity respectively, and they are calculated as follows:

$$k_\sigma = \frac{k_w \rho_w \varepsilon_{bw} + k_{ds}\rho_{ds}\varepsilon_{ds} + k_{PCM}\rho_{PCM}\varepsilon_{PCM} + k_w\rho_w\varepsilon_l}{\rho_w\varepsilon_{bw} + \rho_{ds}\varepsilon_{ds} + \rho_w\varepsilon_l} \tag{1f}$$

$$k_\gamma = \frac{k_v\rho_v + k_a\rho_a}{\rho_v + \rho_a} \tag{1g}$$

where subscripts v and a, refer to the water vapor and air, respectively.

The moisture mass balance in the gas phase is stated as follows:

$$\frac{\partial(\varepsilon_\gamma \bullet \rho_v)}{\partial t} + \frac{\partial}{\partial x}\left(-D_{eff}\frac{\partial \rho_v}{\partial x}\right) + \dot{m}_{gs} + \dot{m}_{gl} = 0 \tag{2a}$$

$$D_{eff} = \frac{\varepsilon_\gamma \bullet D_a}{\tau} \tag{2b}$$

$$D_a = 2.23 \bullet 10^{-5}\left(\frac{T}{273.15}\right)^{1.75} \tag{2c}$$

Assuming no advection and diffusion phenomena, the free liquid water and bounded water balances are stated as follows:

$$\rho_w\frac{\partial \varepsilon_l}{\partial t} = \dot{m}_{gl} - \dot{m}_{ls} \tag{3}$$

$$\rho_w\frac{\partial \varepsilon_{bw}}{\partial t} = \dot{m}_{gs} + \dot{m}_{ls} \tag{4}$$

Water phase change rates are calculated by the following expressions:

$$\dot{m}_{gs} = \frac{8D_f\rho_{ds}}{d_f^2}\left(Regain_{eq} - Regain_f\right) \tag{5a}$$

$$\dot{m}_{gl} = \begin{cases} c \bullet (\rho_v - \rho_{v,sat}) & \rho_{v,sat} \leq \rho_v \\ h_m a_s\frac{\varepsilon_l}{\varepsilon_l^{cr}}(\rho_v - \rho_{v,sat}) & \rho_{v,sat} \geq \rho_v \end{cases} \tag{5b}$$

$$a_s = \frac{4\varepsilon_{ds}}{d_f} \tag{5c}$$

$$\dot{m}_{ls} = h_m a_s \gamma_{ls}\left(\frac{Regain_{eq}}{Regain_f} - 1\right) \tag{5d}$$

$$Regain_f = \frac{\varepsilon_{bw}\rho_w}{\varepsilon_{ds}\rho_{ds}} \tag{5e}$$

Table 4
Properties of skin layers taken from Ref. [8].

Property	Epidermis	Dermis	Subcutaneous
Thermal conductivity (k) W/(m·K)	0.255	0.523	0.167
Specific heat (c_p) J/(kg·K)	3600	3400	3060
Density (ρ) kg/m^3	1200	1200	1000
Thickness (w) mm	0.08	2	10
Blood perfusion rate (G) s^{-1}	1.25×10^{-3}	1.25×10^{-3}	1.25×10^{-3}

Table 5
Initial conditions assumed for the firefighting protective clothing.

Property	Outer shell	Moisture Barrier	Thermal Inner
$\varepsilon_{l,init}$	Distribution (0–0.27) (i.e., dry to saturated)	0	Distribution (0–0.25) (i.e., dry to saturated)
$\varepsilon_{b,init}$	0.025	0.007	0.008
T_{init}	34 °C	34 °C	34 °C
$\varnothing_{init}$	0.65	0.65	0.65

well.

$$\varepsilon_{ds} + \varepsilon_{bw} + \varepsilon_{PCM} + \varepsilon_\gamma + \varepsilon_l = 1 \tag{6}$$

2.3.2. Skin model

The Pennes' bio-heat model is assumed to describe the heat exchanges in the firefighter's skin layers. The following equations describe heat transport in the epidermis, dermis, and subcutaneous:

$$\rho_{ep}C_{ep}\frac{\partial T}{\partial t} = \frac{\partial}{\partial x}\left(k_{ep}\frac{\partial T}{\partial x}\right) \tag{7a}$$

$$\rho_{derm}C_{derm}\frac{\partial T}{\partial t} = \frac{\partial}{\partial x}\left(k_{derm}\frac{\partial T}{\partial x}\right) - G\rho_b c_b(T - T_c) \tag{7b}$$

$$\rho_{subcut}C_{subcut}\frac{\partial T}{\partial t} = \frac{\partial}{\partial x}\left(k_{subcut}\frac{\partial T}{\partial x}\right) - G\rho_b c_b(T - T_c) \tag{7c}$$

where G, ρ_b, c_b and T_c represent the blood perfusion rate, blood density, specific heat, and core body temperature, respectively. The subscripts *ep*, *derm*, and *subcut* stand for epidermis, dermis and subcutaneous, respectively. The properties of the skin layers are shown in Table 4. To note that the blood perfusion rate is assumed constant throughout the simulations. However, it can vary significantly due to vasodilation phenomena [42–44].

Like other studies in the field, Henriques' burn criterion to calculate second-degree burn time was utilized [19,32,45,46]. The criterion consists in the integration of the Arrhenius rate equation with respect to time to calculate the accumulated damage to the skin. A second-degree burn is reached when the integral is unity.

Lastly, the volume fraction constraint now includes the PCM phase as

$$Regain_{eq} = \frac{\varepsilon_{bw}|_{eq} \bullet \rho_w}{\varepsilon_{ds}\rho_{ds}} = 0.578 \bullet Regain_{f(\varnothing=65\,\%)} \bullet \varnothing \bullet \left[(0.321 + \varnothing)^{-1} + (1.262 - \varnothing)^{-1}\right] \tag{5f}$$
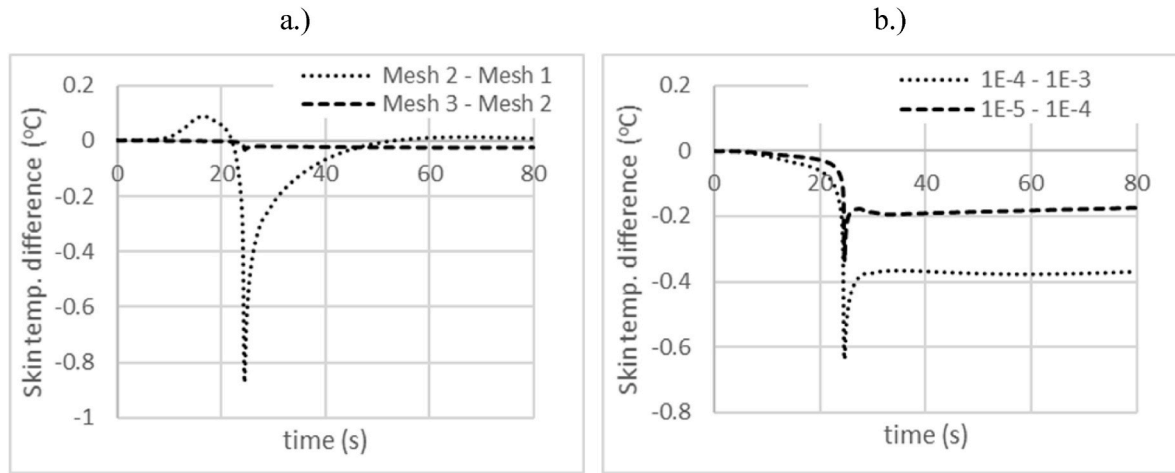
Fig. 2. a.) Differences in the skin temperature obtained for the different meshes b.) Differences in the skin temperature for the different relative tolerances.

Table 6
Meshes used to test for spatial mesh independence.

Mesh no.	Elements in textile layer	Elements in skin layer
Mesh 1	50	5
Mesh 2	500	20
Mesh 3	1000	100

2.4. Boundary and initial conditions

Donnelly et al. [47] divided the firefighting scenario into four thermal classes that a firefighter can face. These classes are categorized based on the heat flux and air temperature. In this work, three heat exposure intensities are considered to simulate high- (84 kW/m^2), medium- (12 kW/m^2), and low-intensity (5 kW/m^2) heat exposure scenarios [17,20,48]. This incoming external heat flux (q_w) is imposed at boundary 1 (Fig. 1) as a Newman condition (equation (8a)).

$$q_w = - k_{eff,outer} \frac{\partial T}{\partial x}\bigg|_{x=0} \tag{8a}$$

Also, at this boundary (1, Fig. 1), water vapor is transferred from the garment to the ambient by convection (equation (8b)), assuming an ambient temperature of 34 °C with 65% R.H.

$$k_c(\rho_v - \rho_{amb}) = - D_{eff,outer} \frac{\partial \rho_v}{\partial x}\bigg|_{x=0} \tag{8b}$$

At boundary 2* (Fig. 1), a continuity and symmetry boundary condition is assumed for the energy and mass balances (equations (8c) and (8d), respectively).

$$-k_{epidermis} \frac{\partial T}{\partial x}\bigg|_{x=L_{outer}+L_{moisture}+L_{inner}} = - k_{eff,inner} \frac{\partial T}{\partial x}\bigg|_{x=L_{outer}+L_{moisture}+L_{inner}} \tag{8c}$$

$$0 = - D_{eff,inner} \frac{\partial \rho_v}{\partial x}\bigg|_{x=L_{outer}+L_{moisture}+L_{inner}} \tag{8d}$$

where L_{outer}, $L_{moisture}$ and L_{inner} represent the outer shell, moisture barrier, and thermal inner widths, respectively.

A constant core body temperature of 37 °C (Dirichlet condition) is considered at boundary 2 of Fig. 1.

It is also assumed that the PCM FPC assembly is initially at a constant temperature of 34 °C, and the skin at a temperature that linearly varies between the epidermis and subcutaneous regions, i.e. between 34 and 37 °C [17,20]. An initial relative humidity of 65% is assumed in the PCM FPC assembly. Initial conditions assumed are shown in Table 5.

Regarding the initial water content present in the different layers of the FPC assembly, they are taken from the experimental work done by Zhang et al. [49]. It is assumed that this initial presence of water can be due to different water source exposures such as sweat and/or hose spraying.
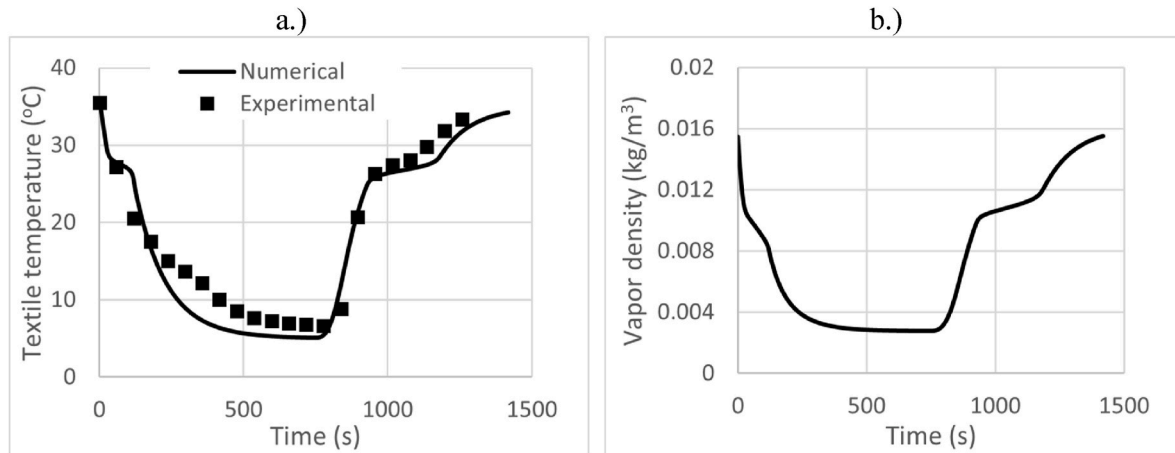
Fig. 3. Comparison between experimental [23] and numerical results for hot and cold chamber experiments to study the thermal properties of a polyester textile incorporated with micro PCMs. a.) Temperature at the center of the textile b.) Vapor density at the center of the textile.
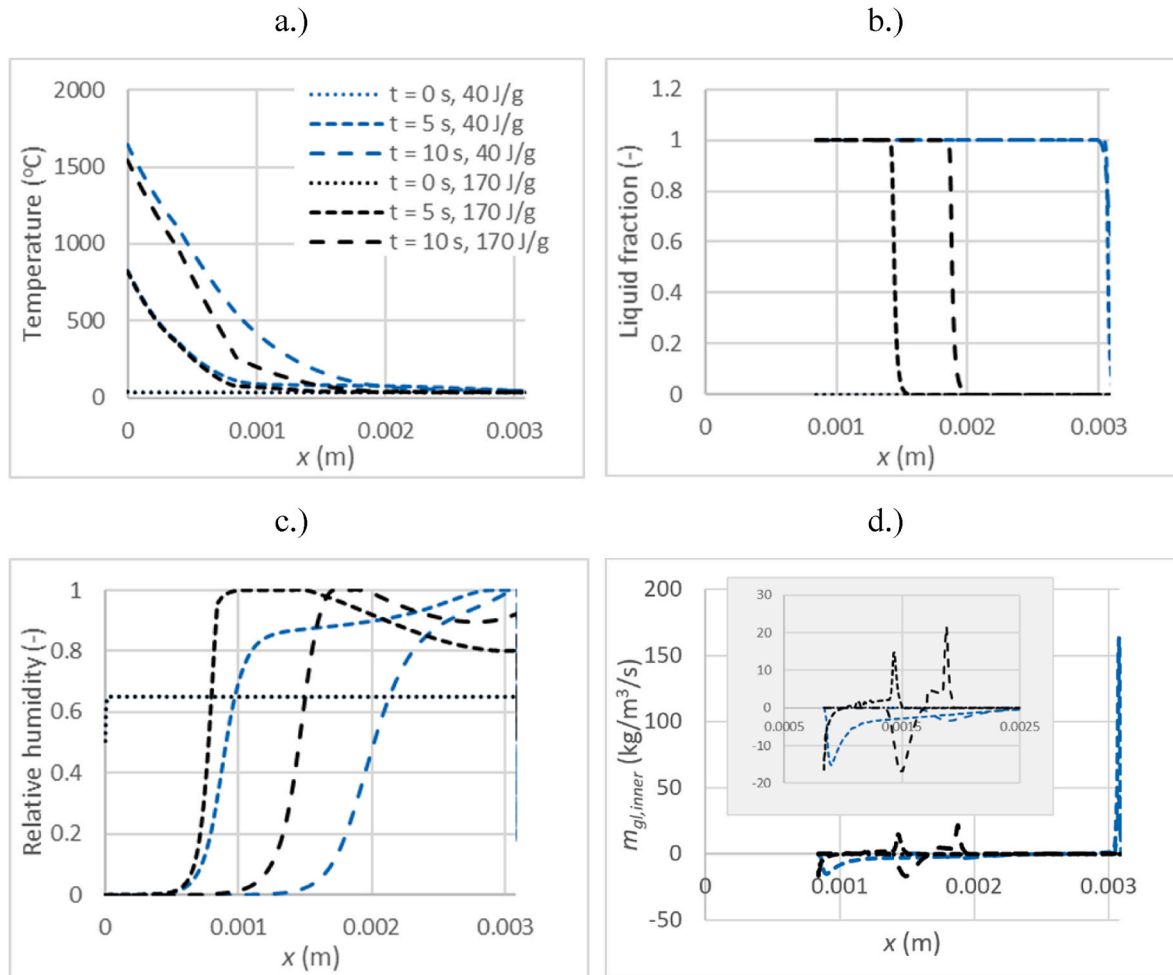
Fig. 4. Calculated properties along the thickness of PCM FPC assembly considering the outer shell initially saturated and different textile latent heats, for an exposure of 84 kW/m², at the indicated times; a.) Temperature profiles, b.) PCM liquid fraction, c.) Relative humidity, and d.) Water vapor condensation rate for thermal inner.

2.5. Numerical methods

Simulations were performed on a FEM platform in a AMD Ryzen Threadripper 3960X 24-Core Processor @3.79 GHz. The shape function type assumed for all PDEs was Langrangian with a quadratic element order concerning the independent spatial variables. A backward differentiation formula of varying order (between 1 and 2) was employed to compute the solution with respect to time. Due to the highly varying magnitudes in the values of the different properties, scale factors were employed so as to promote solution convergence. The scale factors employed for ε_b, ε_g, ε_l, ρ_v and T were 0.01, 0.5, 0.27, 0.1 and 400, respectively.

2.6. Grid independence tests

To ensure solution accuracy and promote computational efficiency, grid independence tests concerning time and space were performed. Fig. 2a shows the difference in skin temperature histories obtained with the different indicated meshes in Table 6. As can be seen, spatial mesh independence is obtained with Mesh 2. A backward differentiation formula solver was used to choose the best time step, utilizing a relative tolerance as a criterion. The best relative tolerance obtained is 10^{-4} and a residual-based termination criterion was utilized (Fig. 2 a and b).

2.7. Model validation

The textile model was validated with the experimental data outlined

in Ref. [23]. Micro PCMs were incorporated in a polyester fabric and their thermoregulatory capabilities were tested by imposing step changes in the ambient temperature to promote their liquefaction/solidification. The PCM used was paraffin. For such, two chambers were conditioned with different temperatures (i.e., 35 °C and 5 °C, corresponding to the hot chamber and cold chamber, respectively) but with an equal relative humidity of 40%. The polyester textile with PCM microcapsules was initially conditioned in the hot chamber. Thus, the PCM was initially in a liquid state. The garment was then moved into the cold chamber and remained there for 816 s, turning the PCM into solid. The textile was then moved back into the hot chamber and remained there for another 600 s.

Fig. 3 shows the obtained experimental and numerical temperature and numerically obtained water vapor density at the center of the textile. As can be seen, good agreement is obtained proving the adequacy of the model to simulate heat and mass transport in textiles incorporating micro encapsulated PCMs. The deviations which exist in the first part of the process (i.e., Fig. 3, $t < 816$ s) are due to hysteresis phenomena regarding the phase change of the PCM, an effect neglected in the current model. The vapor density trends obtained are as expected since water vapor adsorbs in the fiber and condenses for lower textile temperatures, whilst the opposite is true for higher textile temperatures.

2.8. PCM selection criteria

PCM selection criteria have been proposed in previous works to incorporate PCMs in dry FPCs [17]. There, it was determined that the
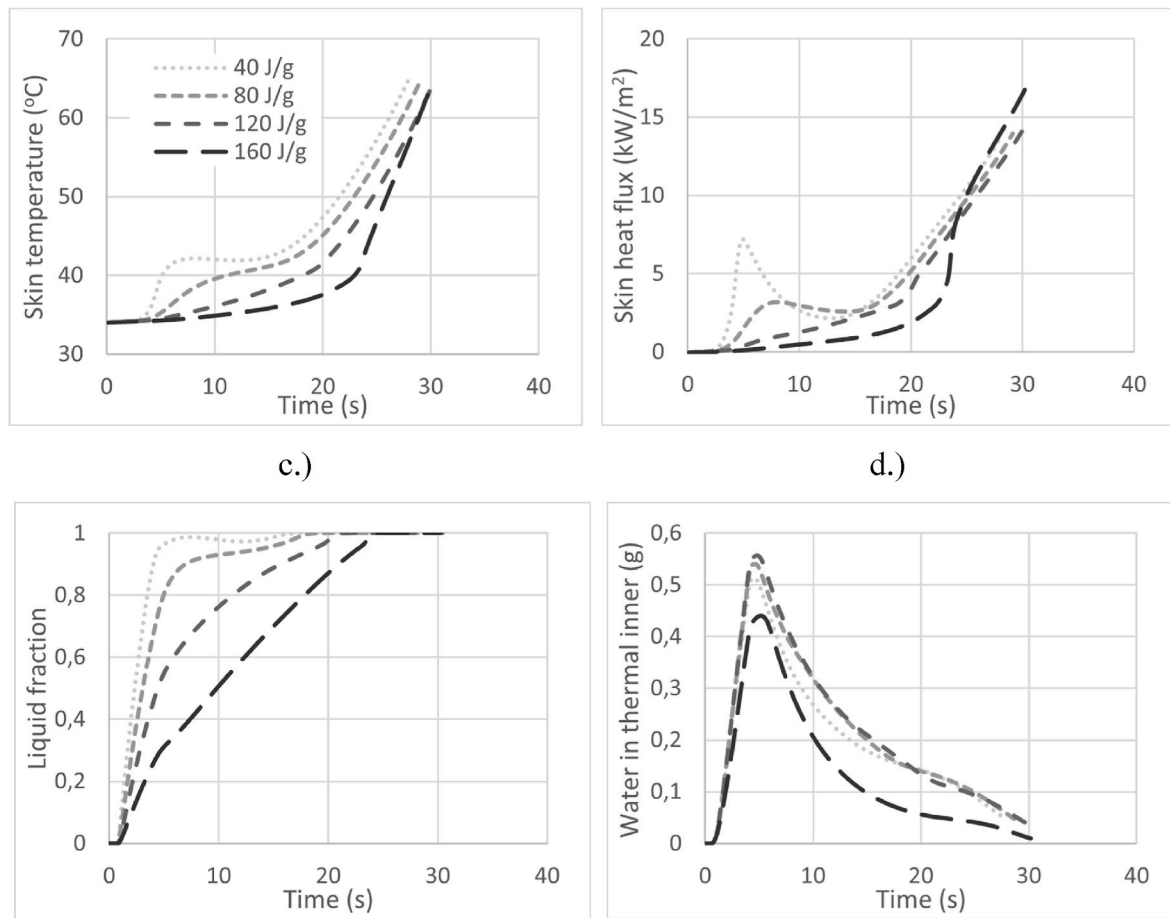
Fig. 5. a.) Skin temperature, b.) Skin heat fluxes, and c.) PCM liquid fraction and d.) Thermal inner water content histories for the indicated thermal inner textile latent heats; for a high-intensity heat exposure (84 kW/m²).

significant variables to consider in PCM selection are its melting temperature, latent energy, and exposure scenario. A PCM with a substantially high melting temperature may only melt partially before the firefighter experiences a second-degree burnout, thus the PCM not being efficient. Also, if the PCM disposes of insufficient latent energy, the increase in second-degree burnout time might not be significant. In this study, new PCM selection criteria for wet PCM FPCs will be established in function of the PCMs melting temperature and latent energy for high-, medium-, and low-intensity exposures.

3. Results

When a PCM FPC assembly is exposed to a given heat flux, the PCM will tend to melt, originating lower temperatures in the garment and thus at the firefighters skin [17,19–21,48]. This happens because part of the incoming dry heat from the flame accumulates as latent heat in the PCM [17]. However, when a PCM is present in the thermal inner of a wet FPC assembly, in some cases, the PCM might melt due to latent heat absorption associated with vapor re-condensation. An example of such a case is shown in detail in Fig. 4.

Fig. 4a shows the temperature profiles obtained after a 0, 5 and 10 s exposure to an 84 kW/m² heat flux when the outer shell of the PCM FPC assembly is initially saturated with water. Two thermal inner layers with different PCM textile latent heats are considered in Fig. 4. As expected, the incorporation of a significant textile latent heat originates lower temperature along the firefighting protective clothing [17]. However, the addition of a greater textile fiber latent heat means that more PCM is present in the thermal inner, and thus it takes more time and energy to melt (e.g. Fig. 4b, $t = 5$ s, 170 J/g, x ≈ 0.0015 m vs. $t = 5$ s, 40 J/g, x ≈

0.003 m). As it takes more time, the water vapor generated at the outer shell may diffuse and reach the thermal inner where solid PCM is still present (e.g. Fig. 4b, $t = 5$ s, 0.0015 m $< x <$ 0.003 m). The melting thus either may occur as a result from the accumulation of energy directly coming from the flame, or due to the latent heat liberated by the re-condensation of water vapor arriving at the thermal inner in the positions where solid PCM is present. This is evidenced by the relative humidity registered close to the positions where PCM melting occurs as its value is unity implying water re – condensation near those positions of the textile (e.g. Fig. 4c, $t = 5$ s, 170 J/g, 0.0008 m $< x <$ 0.0016 m). This is further confirmed by the water vapor condensation rates at the same positions where the PCM is melting (e.g. Fig. 4d, $t = 5$ s, 170 J/g, x ≈ 0.0015 m). Notice that by incorporating a significant textile latent heat, vapor re-condensation at the skin is prevented (Fig. 4d, $x = 0.003$ m).

Thus, in an effort to find in what conditions the phenomena described above happen, in this work, different textile latent heats, PCM properties, exposure heat fluxes and initial water distributions in the PCM FPC assembly are considered. For each set of parameters, second-degree burn time tendencies are computed and discussed in light of the phenomena outlined above. More concretely, in the first section, textile latent heat is varied for constant PCM properties and initially saturated outer shell. In the second section, PCM properties are varied, and the thermal inner or outer shell are considered initially saturated. Lastly, in the third section, similarly to the second section, the PCM properties are also varied, but both layers are considered to be simultaneously initially wet. High –, medium – and low – intensity heat exposures are considered in each of the sections.

a.)   b.)
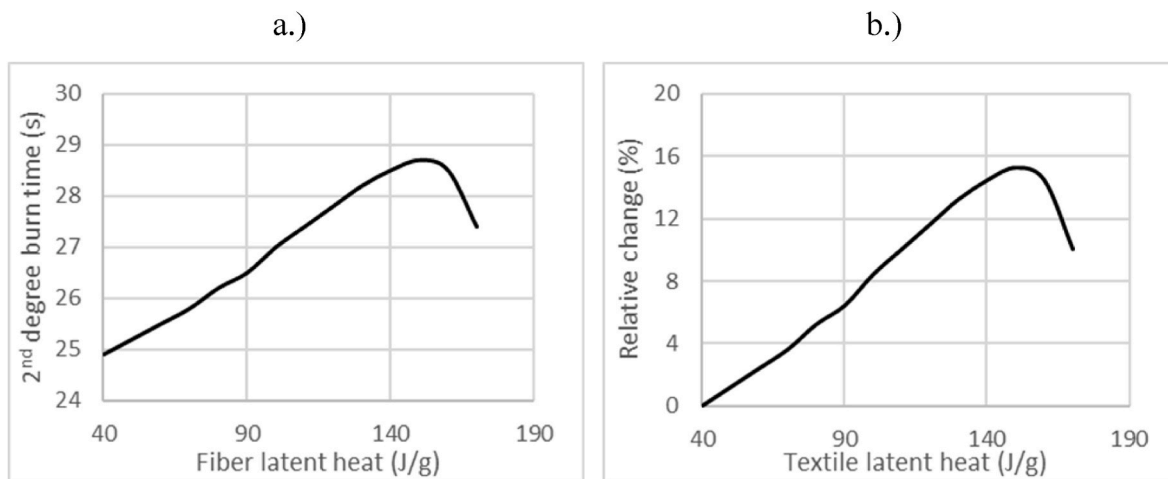
Fig. 6. a.) Second-degree burn time variance with textile latent heat b.) Relative change in second-degree burn time with textile latent heat; for a high-intensity heat exposure (84 kW/m^2).

a.)   b.)

c.)   d.)
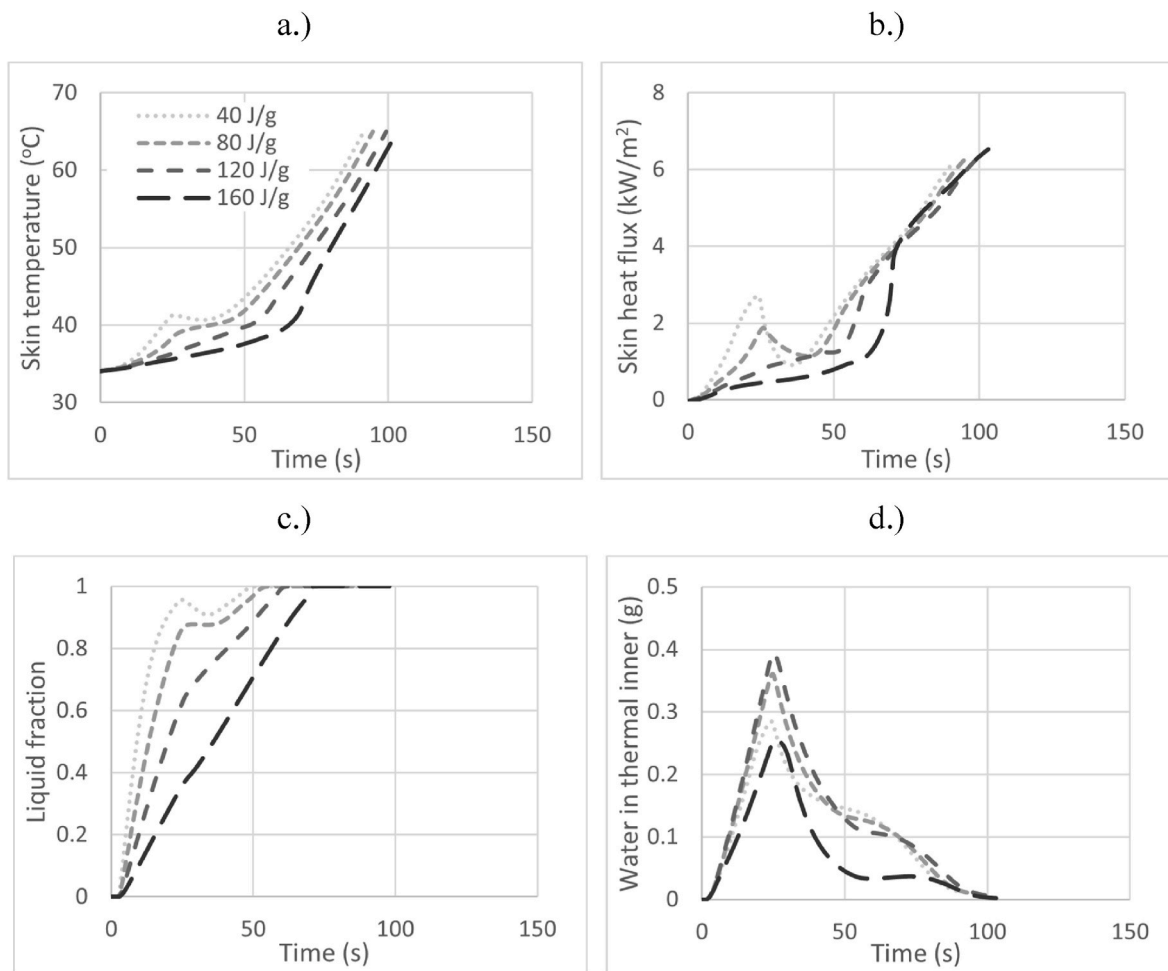
Fig. 7. a.) Skin temperature, b.) Skin heat fluxes, and c.) PCM liquid fraction histories obtained for the indicated thermal inner textile latent heats; for a medium – intensity heat exposure (12 kW/m^2).

3.1. Influence of textile latent heat

As discussed in previous papers, increasing the PCM mass (and consequently the textile latent heat) in a dry firefighting garment greatly increases the thermal performance of such [17,50]. However, when free water is present in the outer shell (i.e. assumed saturated), associated evaporation and condensation phenomena in the assembly will alter the PCMs melting behavior, and thus the necessary textile latent heat to provide enough protection to the firefighter [17].

Fig. 5a shows the skin temperature histories obtained for an exposure

a.)

b.)
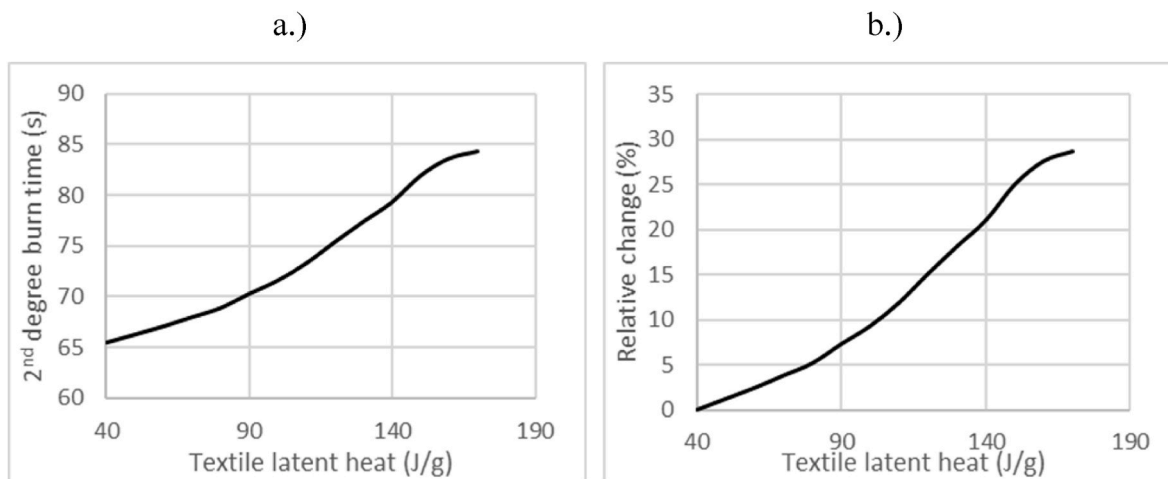
Fig. 8. a.) Second-degree burn time variance with textile latent heat b.) Relative change in second-degree burn time with textile latent heat; for a medium-intensity heat exposure (12 kW/m^2).

a.)

b.)

c.)

d.)
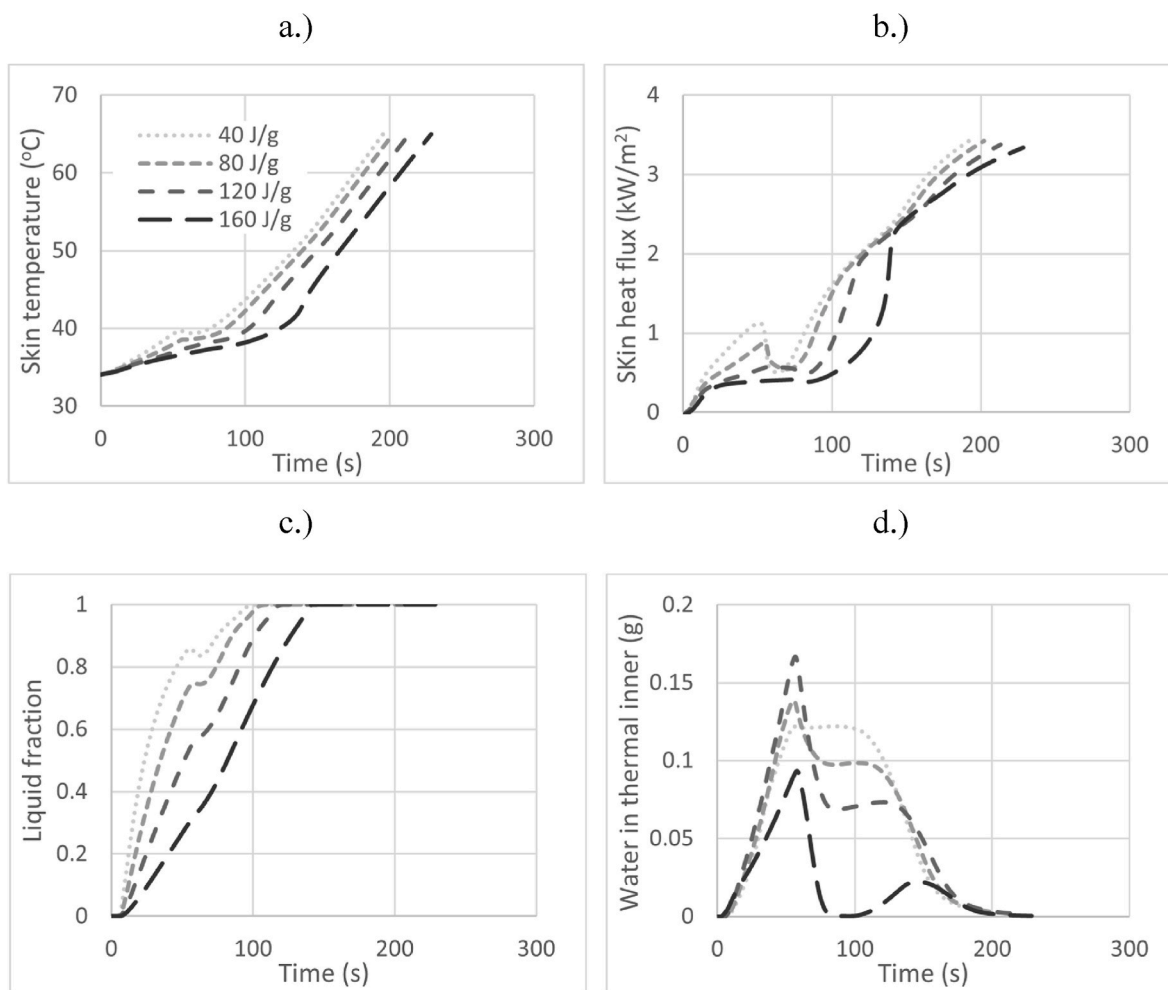
Fig. 9. a.) Skin temperature b.) Skin heat fluxes and c.) PCM liquid fraction histories for the indicated thermal inner textile latent heats; for a low-intensity heat exposure (5 kW/m^2).

intensity of 84 kW/m^2 for various thermal inner textile latent heats. For exposure times less than 20 s, an increase in textile latent heat originates a decrease in the skin temperature. This is consistent with the decreasing skin heat fluxes obtained (Fig. 5b). During this period, the water present in the outer shell vaporizes and migrates towards the thermal inner and

the skin. It then re-condenses (Fig. 5d), releasing latent heat to the surroundings. This explains the sudden skin temperature spike registered in the beginning (e.g., Fig. 5a, $t = 6.1$ s, 40 J/g). For higher textile latent heats this tends not to happen, as greater amounts of PCM promote more vapor re-condensation at positions in the thermal inner
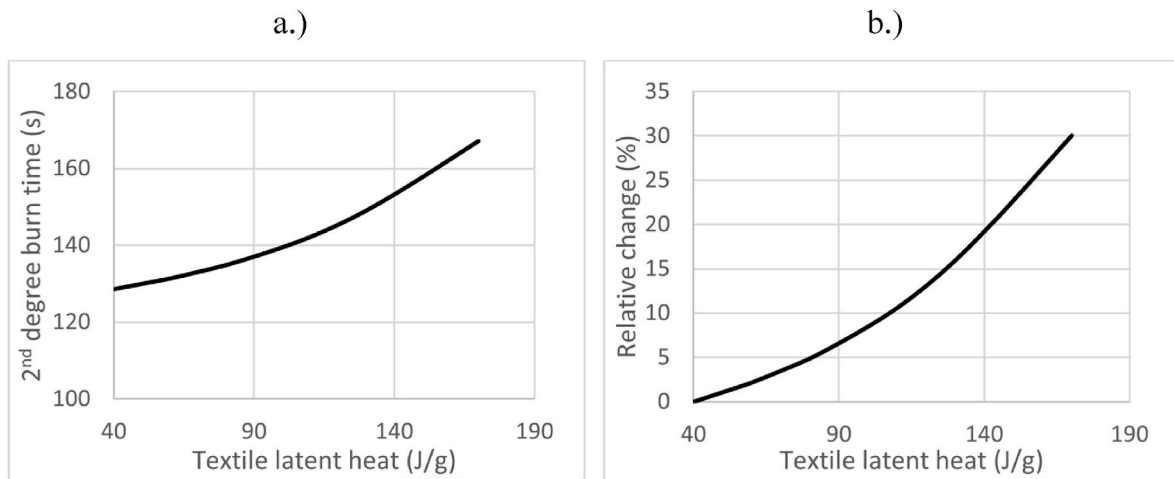
Fig. 10. a.) Second-degree burn time variance with textile latent heat b.) Relative change in second-degree burn time with the textile latent heat; for a low-intensity heat exposure (5 kW/m^2).
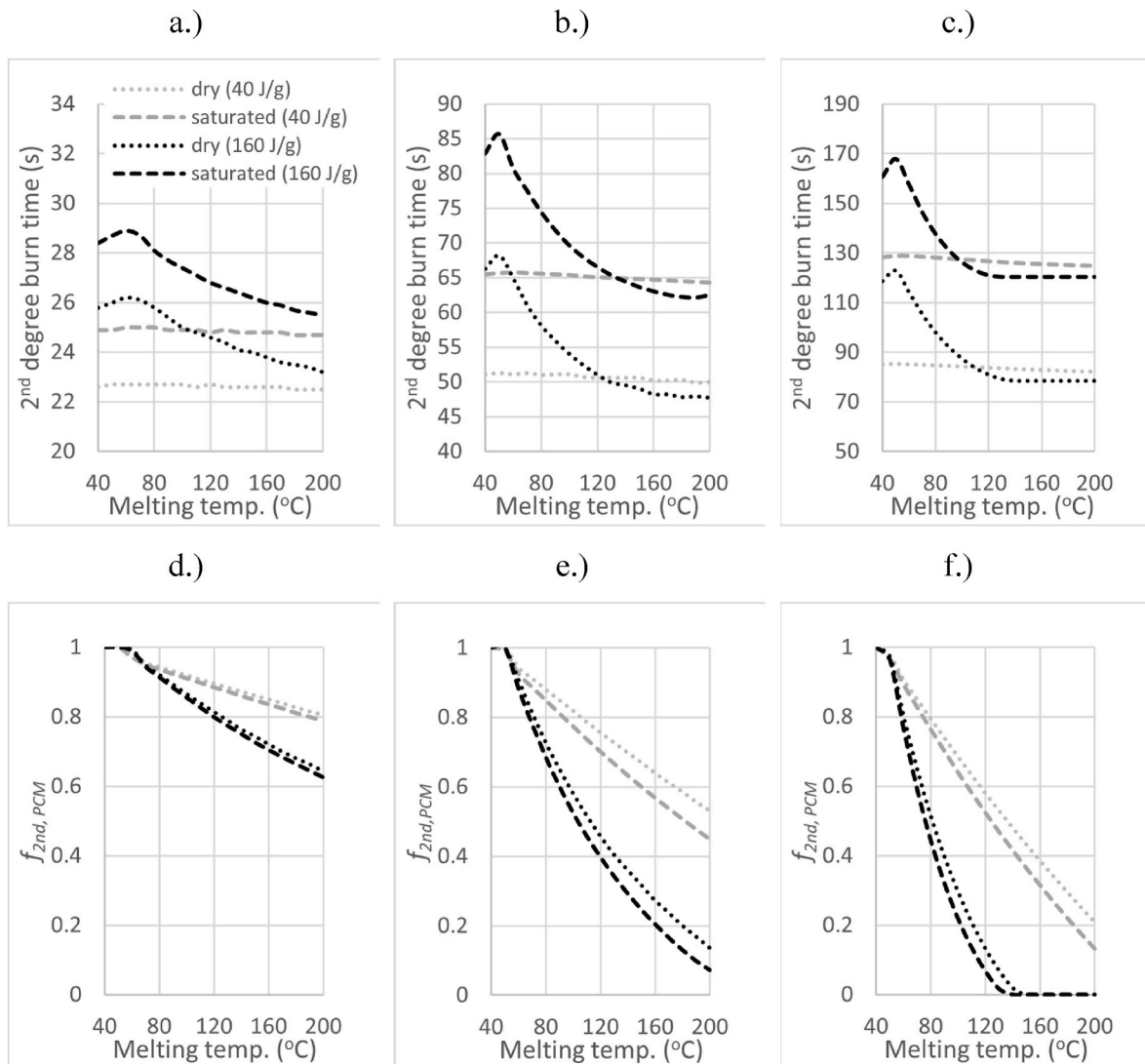
Fig. 11. Second-degree burn times for the indicated PCM melting temperature and textile latent heats for cases where the outer shell is dry or saturated for: a.) High, b.) Medium, and c.) Low–intensity exposures. PCM liquid fraction at second-degree burnout time ($f_{2nd, PCM}$) for the indicated PCM melting temperature and textile latent heats for cases where outer shell is dry or saturated for d.) High, e.) Medium, and f.) Low-intensity exposures.
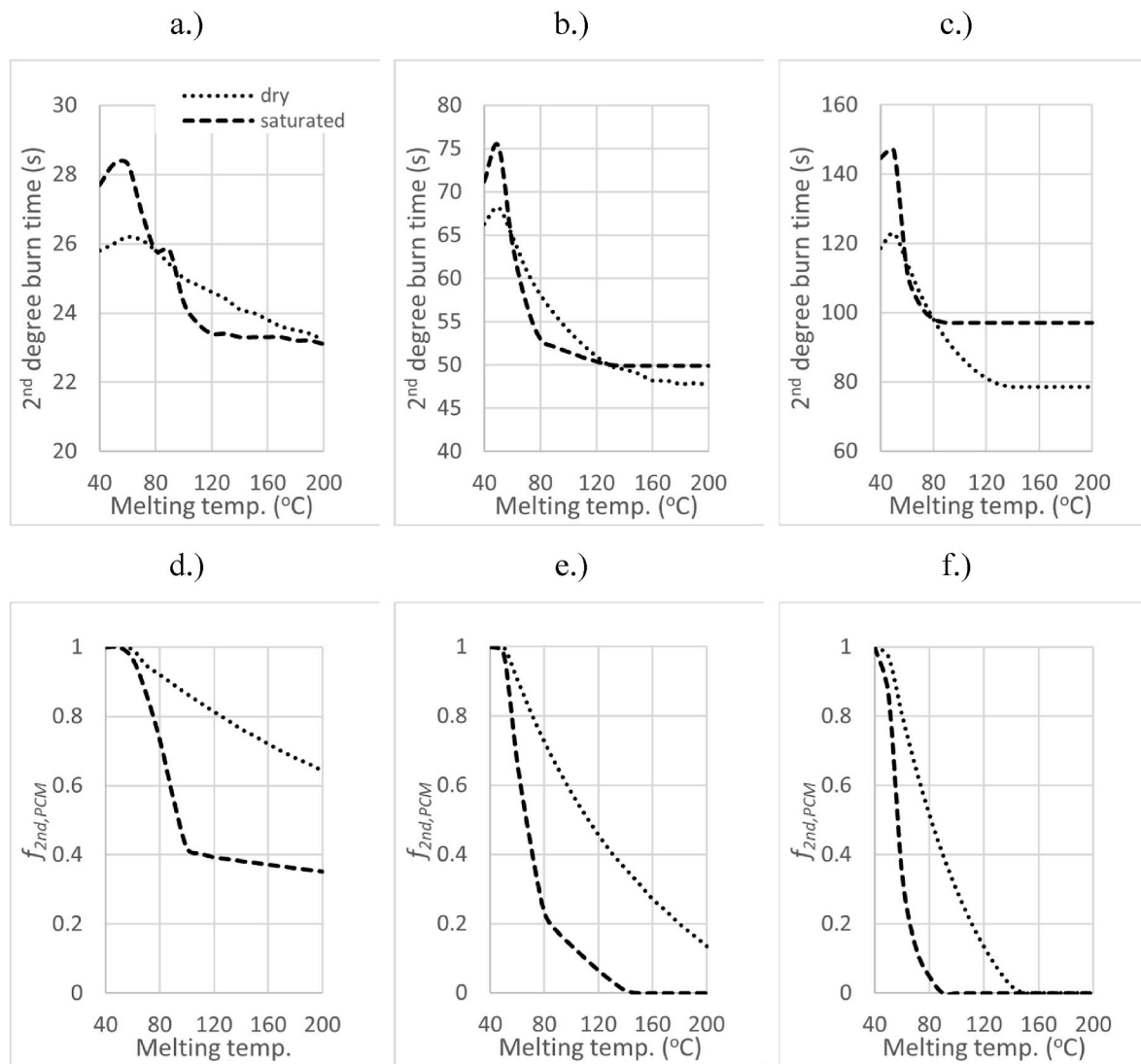
Fig. 12. Second-degree burn times for the indicated PCM melting temperature and a 160 J/g textile latent heat for cases where the thermal inner is dry or saturated for a.) high, b.) medium, and c.) low-intensity exposures. PCM liquid fraction at second-degree burnout time ($f_{2nd,\,PCM}$) for the indicated PCM melting temperature and a 160 J/g textile latent heat for cases where the thermal inner is dry or saturated for d.) high e.) medium and f.) low-intensity exposures.

further away from the skin, thus mitigating re – condensation at the skin (i.e. Fig. 4). The latent heat liberated by the vapor re-condensation only melts part of the PCM in the thermal inner if significant textile latent heats are considered (e.g., Fig. 5c, $t = 6.1$ s, 160 J/g). The re-condensed water in the thermal inner then keeps re-evaporating and re-condensing mostly at positions where textile latent heat (i.e. solid PCM) is present until all PCM is liquefied (i.e. Fig. 5c, *Liquid fraction* = 1). A sudden increase in skin temperature and heat flux is then registered due to vapor re-condensation directly at the skin (e.g. Fig. 5a, b and c, 21.6 s $< t <$ 24.2 s, 160 J/g). Bulky thermal inners tend to have low porosities which inhibit the accumulation of water. Such causes them to have higher thermal diffusivities. This explains the higher skin temperatures and skin heat fluxes obtained after the PCM in the thermal inner has melted (e.g. Fig. 5a and b, $t > 21.6$ s, 160 J/g). Thus, for high – intensity exposures, the presence of greater textile latent heat delays the condensation of water vapor at the skin due to PCM phase change. How this impacts second – degree burn time tendencies is shown in Fig. 6.

A positive almost linear trend is observed up to a textile latent heat of 150 J/g, followed by a decline in the thermal performance due to the higher thermal inner thermal diffusivity. Therefore, the incorporation of textiles with higher latent heats promotes thermal performance, even under wet conditions where steam condensation is present (Fig. 4).

However the mechanism by which such is accomplished is different from a dry PCM FPC assembly.

For medium – intensity exposures, skin temperatures and heat fluxes obtained are of a lesser magnitude with time due to lower heat flux exposure intensity (Fig. 7a and b). Skin heat flux spikes associated to water condensation at the skin tend to be less intense, especially for thermal inners with lower textile latent heats . For lower intensity heat exposures, less water vapor diffuses towards the thermal inner and hence a lower textile latent heat is needed to fully re – condense it (Fig. 7d). Some thermal inners still have substantial unused latent heat (i.e. solid PCM) after re-condensation of water coming from the outer shell (i.e. Fig. 7a, $t \approx 25$ s, *textile latent heat* > 80 J/g).

Second – degree burn time tendencies are similar to the case of higher intensity exposures (Fig. 8a and b). Differences in thermal diffusivities of the PCM thermal inners are reduced due the lesser presence of water. Hence, second degree burn times do not drop substantially even when very large quantities of PCM are incorporated (i.e. Fig. 8a and b, *Textile latent heat* > 150 J/g).

For low-intensity exposures, the spike in skin temperatures and heat fluxes is small, and its intensity almost varies proportionally to the textile latent heat (Fig. 9a and b). For all textile latent heats considered, the PCM does not fully melt after re – condensing the incoming water
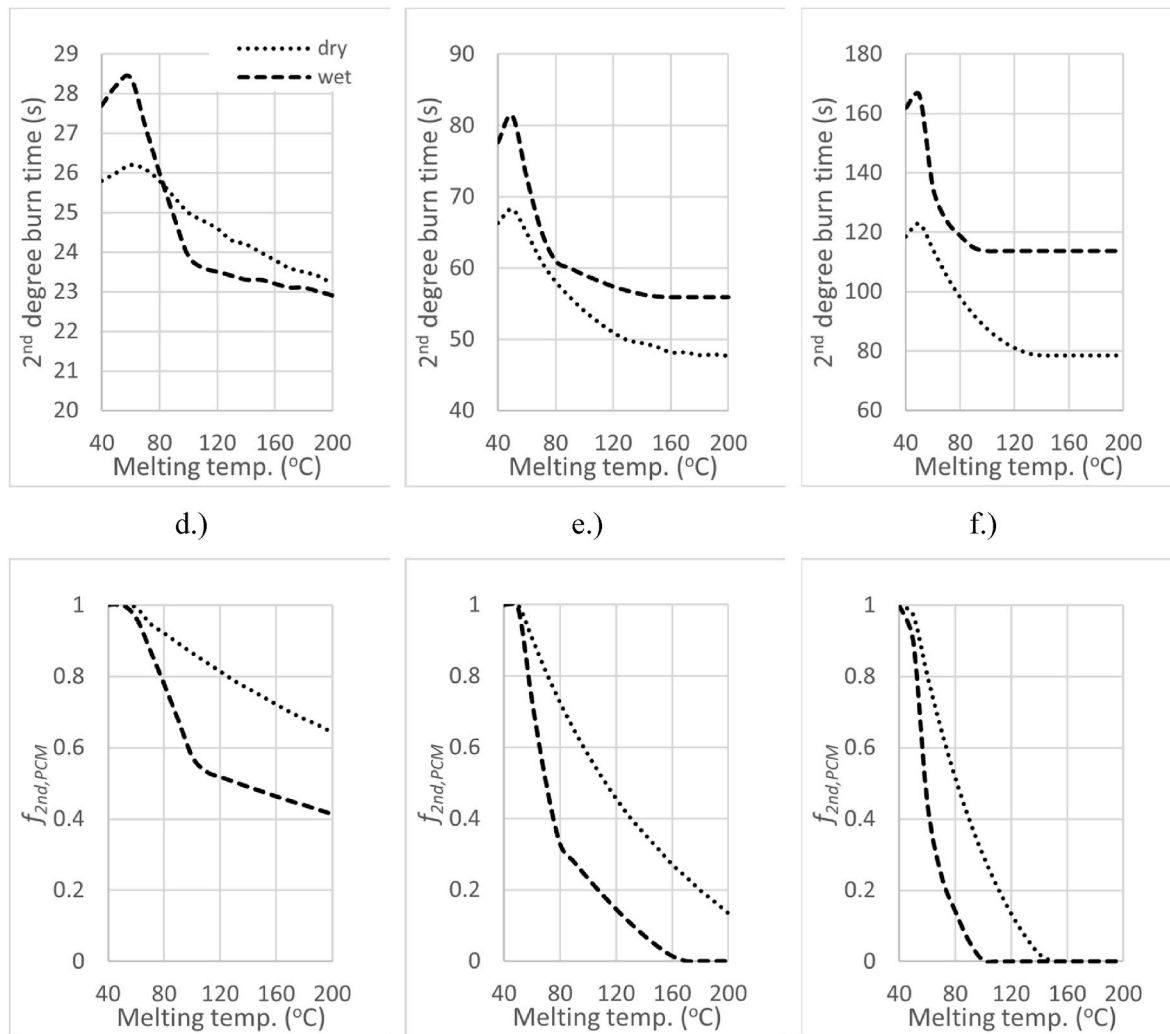
Fig. 13. Second-degree burn times for the indicated PCM melting temperature and a 160 J/g textile latent heat for cases where thermal inner and outer shell are at a 50% saturation wetness level for a.) high, b.) medium, and c.) low-intensity exposures. PCM liquid fraction at second degree burnout time ($f_{2nd,PCM}$) for the indicated PCM melting temperature and a 160 J/g textile latent heat for cases where thermal inner and outer shell are at a 50% saturation wetness level for d.) high, e.) medium, and f.) low-intensity exposures.

vapor from the outer shell (Fig. 9c). However, small quantities of water vapor diffuse towards the skin as not all re-condenses at the PCM. Less bulky PCM thermal inners allow for greater vapor diffusion towards the skin due to their higher porosities and faster melting. To note that for very high textile latent heats, during the exposure, the PCM thermal inner dries out, and thus PCM consumption rate increases (i.e. Fig. 9c and d, 80 s < t < 110 s, 160 J/g). This does not tend to happen in other exposure scenarios. Second-degree burn times obtained for low-–intensity exposures tend to vary quasi–linearly with textile latent heat (Fig. 10a and b).

Bulkier thermal inners with higher textile latent heats will delay second–degree burn occurrence except for high-intensity exposures when the textile latent heat incorporated is very significant. It is also important to point out that current PCM microencapsulation methods only allow for textile latent heats surrounding the 40 J/g mark, which is clearly insufficient to provide the firefighter with any significant protection.

3.2. Effect of water distribution on PCM selection

The incorporated PCM in the PCM FPC assembly promotes water vapor condensation, if its melting temperature is low enough. The range

of melting temperatures which promote vapor condensation depend on the initial water distribution in the PCM FPC, as well as the heat exposure intensity. Lower melting temperatures promote more water vapor condensation and thus higher second – degree burn time windows.

3.2.1. Water presence in the outer shell

Fig. 11a–c shows the second-degree burn times for different heat exposure intensities and different PCM melting temperatures, considering a dry or saturated outer shell and an inner layer with different textile latent heat. As shown, independently of the textile latent heats considered, differences in second-degree burn time exist whether the outer shell is dry or saturated. Higher second-degree burn times are obtained when the outer shell is saturated for all PCM melting temperatures considered. For example, consider a PCM FPC assembly with a textile latent heat of 160 J/g incorporating a PCM with a melting temperature of 80 °C. If its outer shell is initially dry, the second-degree burnout obtained when exposed to a high heat exposure is 24.5 s, but if it is initially wet and fully saturated, it increases up to 27.6 s (Fig. 11a). Furthermore, similar increases in second-degree burn time also occur if other PCM melting temperatures are considered. Hence, for high-–intensity exposures, the increase in second-degree burn time due to water presence in the outer shell of a PCM FPC assembly, is practically

independent of the PCM textile latent heat, and its melting temperature. The registered PCM liquid fractions at second-degree burn time for dry and wet PCM FPC assemblies evidence why this is so (Fig. 11d–f). As shown, the PCM liquid fractions registered at the second-degree burn time (i.e. used textile latent heat) do not vary much between the saturated and dry cases. Hence, the influence of PCM melting on second-degree burn time of a PCM FPC is the same, regardless of whether the outer shell is wet or dry. The adequate PCM selection is dependent on other variables that have been explored in other studies in the literature where the PCM FPC assembly suit was considered dry [17,50].

3.2.2. Water presence in the thermal inner

For a PCM FPC assembly with an initial wet thermal inner, PCMs with higher melting temperatures are unable to promote steam re-condensation, promoting the fast occurrence of second-degree burns. This is essentially true for high-intensity exposures (Fig. 12a). For initially wet PCM thermal inner, the second-degree burn time tendency is characterized by a steep decline with PCM melting temperature (i.e. Fig. 12a, 40 °C < *Melting temp.* < 110 °C) followed by a much shallower decline (i.e. Fig. 12a, *Melting temp.* ≥ 110 °C). When PCM melting temperature is low, increasing it will decrease the amount of re-condensed water at the PCM thermal inner. This is because a higher PCM melting temperature implies higher temperatures in the PCM FPC assembly [51]. The water vapor diffuses and re-condenses at the skin, spiking skin temperature rise. Consequently, the PCM has less time to fully melt before a second-degree burn is registered, thus explaining its increasing partial melting with increasing melting temperature (i.e. Figs. 12d, 40 °C < *Melting temp.* < 110 °C). When the PCM is unable to condense any of the water, its latent energy is directly utilized to absorb sensible heat from the heat exposure (Fig. 12a, *Melting temp.* ≥ 110 °C). Similar phenomena occur for medium – intensity exposures where PCMs with melting temperatures lesser than 80 °C promote steam re-condensation in the thermal inner (Fig. 12b and e). For low – intensity exposures, steam re-condensation always occurs at the thermal inner for all PCM melting temperatures where PCM liquefaction is observed. Hence the tendencies observed (Fig. 12c and f), which are similar to tendencies for a wet outer shell (Fig. 11). In such cases steam re-condensation in the thermal inner was also always verified.

Thus, presence of water in the thermal inner impacts PCM selection greatly, depending on the objective of the incorporation of such. PCMs with low melting temperatures are recommended for protection against scald burns, whilst the opposite is recommended to solely store sensible heat from the heat exposure.

3.2.3. Water presence in the outer shell and thermal inner

Simultaneous presence of water in the outer shell and thermal inner is likely due to external (e.g., hose spraying) and internal (e.g., perspiration) moisture sources. When water is present in both layers, second-degree burn time tendencies are mainly influenced by water in the thermal inner (i.e. similar tendencies between Figs. 12 and 13).

Fig. 13 shows the variance of second-degree burn time and PCM liquid fraction at that time with melting temperature for high, medium, and low-intensity exposures. The wet case refers to a 50% saturation level both in the outer shell and thermal inner. The tendencies of second-degree burn time and PCM liquid fraction (Fig. 13) are comparable with the results obtained when only the inner layer is saturated, with a wetness level of 100% (Fig. 12). The second-degree burn times obtained are higher, which is in alignment with the higher PCM melting fractions obtained at that time.

4. Conclusions

In this study, the effect of the presence of free water in a PCM FPC assembly was analyzed. At first, the effect of incorporating the thermal inner with different PCM masses was studied for high- (84 kW/m^2), medium- (12 kW/m^2) and low-intensity (5 kW/m^2) heat exposure scenarios. Such was done assuming an initially saturated outer layer. Then, the influence of PCM melting temperature on second-degree burn time was studied considering a wet outer shell and/or thermal inner. The following major conclusions were obtained:

- Independently of the heat exposure scenario considered, incorporating PCMs through micro or nanoencapsulation configures the textile with insufficient PCM mass to benefit second-degree burn time significantly.
- When water is present in the outer shell, part of the steam that diffuses in the direction of the skin re - condenses due to the presence of the PCM. Hence, the PCMs latent heat is used to absorb heat of condensation.
- Also, PCM choice does not change the influence of outer shell water presence on second-degree burn time. Whether free water is present in the outer shell or not, a PCM may be selected independently of such.
- This is not the case when free water is present in the thermal inner, as such results in higher water vapor fluxes towards the skin. In such a case, the PCMs will demonstrate significant partial melting phenomena for all exposure scenarios. If the role of the PCM is to protect the firefighter from dry incoming heat flux, then the presence of steam dramatically decreases the efficiency of the PCMs. In order to eliminate the partial melting phenomena, water vapor management solutions need to be included in the PCM FPC assembly.
- When free water is present in the outer shell and thermal inner, water in the thermal inner tends to determine the efficacy of the PCM in increasing second-degree burn time.

This study intends to highlight how the presence of free water in the PCM FPC assembly may impact the PCMs thermal performance. It will help in the adequate choice of a PCM and guide PCM FPC design when the presence of free water is to be considered.

Declaration of competing interest

The authors declare that they have no known competing financial interests or personal relationships that could have appeared to influence the work reported in this paper.

Data availability

Data will be made available on request.

Acknowledgments

References

[1] R.L. Barker, C. Guerth-Schacher, R.V. Grimes, H. Hamouda, Effects of moisture on the thermal protective performance of firefighter protective clothing in low-level radiant heat exposures, Textil. Res. J. 76 (2006) 27–31, https://doi.org/10.1177/0040517506053947.

[2] Y. Su, J. Li, G. Song, The effect of moisture content within multilayer protective clothing on protection from radiation and steam, Int. J. Occup. Saf. Ergon. 24 (2018) 190–199, https://doi.org/10.1080/10803548.2017.1321890.

[3] C. Keiser, C. Becker, R.M. Rossi, Moisture transport and absorption in multilayer protective clothing fabrics, Textil. Res. J. 78 (2008) 604–613, https://doi.org/10.1177/0040517507081309.

[4] M. Guan, S. Annaheim, M. Camenzind, J. Li, S. Mandal, A. Psikuta, R.M. Rossi, Moisture transfer of the clothing–human body system during continuous sweating under radiant heat, Textil. Res. J. 89 (2019) 4537–4553, https://doi.org/10.1177/0040517519835767.

[5] C. Keiser, R.M. Rossi, Temperature analysis for the prediction of steam formation and transfer in multilayer thermal protective clothing at low level thermal radiation, Textil. Res. J. 78 (2008) 1025–1035, https://doi.org/10.1177/0040517508090484.

[6] C. Keiser, P. Wyss, R.M. Rossi, Analysis of steam formation and migration in firefighters' protective clothing using x-ray radiography, Int. J. Occup. Saf. Ergon. 16 (2010) 217–229, https://doi.org/10.1080/10803548.2010.11076839.

[7] S. Mandal, G. Song, F. Gholamreza, A novel protocol to characterize the thermal protective performance of fabrics in hot-water exposure, J. Ind. Textil. 46 (2016) 279–291, https://doi.org/10.1177/1528083715580522.

[8] P. Chitrphiromsri, Modeling of Thermal Performance of Firefighter Protective Clothing during the Intense Heat Exposure, NCSW, 2004.

[9] P.W. Gibson, Multiphase Heat and Mass Transfer through Hygroscopic Porous Media with Applications to Clothing Materials, 1996.

[10] D. Huang, S. He, Influence of initial moisture content on heat and moisture transfer in firefighters' protective clothing, Sci. World J. 2017 (2017), https://doi.org/10.1155/2017/9365814.

[11] Y. Su, R. Li, G. Song, J. Li, C. Xiang, Modeling steam heat transfer in thermal protective clothing under hot steam exposure, Int. J. Heat Mass Tran. 120 (2018) 818–829, https://doi.org/10.1016/j.ijheatmasstransfer.2017.12.074.

[12] Y. Su, J. Li, X. Zhang, A Coupled Model for Heat and Moisture Transport Simulation in Porous Materials Exposed to Thermal Radiation, Transport in Porous Media, 2019, https://doi.org/10.1007/s11242-019-01347-2.

[13] H. Zhang, G. Song, H. Su, H. Ren, J. Cao, An exploration of enhancing thermal protective clothing performance by incorporating aerogel and phase change materials, Fire Mater. 41 (2017) 953–963, https://doi.org/10.1002/fam.2435.

[14] L. Wang, Y. Lu, J. He, On the effectiveness of temperature-responsive protective fabric incorporated with shape memory alloy (SMA) under radiant heat exposure, Cloth. Text. Res. J. 38 (2020) 212–224, https://doi.org/10.1177/0887302X19892095.

[15] A. Šalej Lah, P. Fajfar, G. Kugler, T. Rijavec, A NiTi alloy weft knitted fabric for smart firefighting clothing, Smart Mater. Struct. 28 (2019), https://doi.org/10.1088/1361-665X/ab18b9.

[16] A. Dąbrowska, G. Bartkowiak, R. Kotas, Evaluation of functionality of warning system in smart protective clothing for firefighters, Sensors 21 (2021) 1–14, https://doi.org/10.3390/s21051767.

[17] A. Fonseca, T.S. Mayor, J.B.L.M. Campos, Guidelines for the specification of a PCM layer in firefighting protective clothing ensembles, Appl. Therm. Eng. 133 (2018) 81–96, https://doi.org/10.1016/j.applthermaleng.2018.01.028.

[18] F.L. Zhu, Q.Q. Feng, R.T. Liu, B.G. Yu, Y. Zhou, Enhancing the thermal protective performance of firefighters' protective fabrics by incorporating phase change materials, Fibres Text. East. Eur. 23 (2015) 68–73.

[19] Y. Su, W. Zhu, M. Tian, Y. Wang, X. Zhang, J. Li, Intelligent bidirectional thermal regulation of phase change material incorporated in thermal protective clothing, Appl. Therm. Eng. 174 (2020), 115340, https://doi.org/10.1016/j.applthermaleng.2020.115340.

[20] H. Phelps, H. Sidhu, A mathematical model for heat transfer in fire fighting suits containing phase change materials, Fire Saf. J. 74 (2015) 43–47, https://doi.org/10.1016/j.firesaf.2015.04.007.

[21] Y. Hu, D. Huang, Z. Qi, S. He, H. Yang, H. Zhang, Modeling thermal insulation of firefighting protective clothing embedded with phase change material, Heat Mass Tran. 49 (2012) 567–573, https://doi.org/10.1007/s00231-012-1103-x.

[22] A. Fonseca, S.F. Neves, J.B.L.M. Campos, Thermal performance of a PCM firefighting suit considering transient periods of fire exposure, post – fire exposure and resting phases, Appl. Therm. Eng. 182 (2020), 115769, https://doi.org/10.1016/j.applthermaleng.2020.115769.

[23] F. Li, L. Yi, A computational analysis for effects of fibre hygroscopicity on heat and moisture transfer in textiles with PCM microcapsules, Model. Simulat. Mater. Sci. Eng. 15 (2007) 223–235, https://doi.org/10.1088/0965-0393/15/3/003.

[24] M. Itani, N. Ghaddar, K. Ghali, Innovative PCM-desiccant packet to provide dry microclimate and improve performance of cooling vest in hot environment, Energy Convers. Manag. 140 (2017) 218–227, https://doi.org/10.1016/j.enconman.2017.03.011.

[25] X. Wan, F. Wang, Udayraj, Numerical analysis of cooling effect of hybrid cooling clothing incorporated with phase change material (PCM) packs and air ventilation

[26] M. Zhao, C. Gao, F. Wang, K. Kuklane, I. Holmér, J. li, The torso cooling of vests incorporated with phase change materials: a sweat evaporation perspective, Textil. Res. J. 83 (2013) 418–425, https://doi.org/10.1177/0040517512460294.

[27] K. Iqbal, A. Khan, D. Sun, M. Ashraf, A. Rehman, F. Safdar, A. Basit, H.S. Maqsood, Phase change materials, their synthesis and application in textiles—a review, J. Textil. Inst. 110 (2019) 625–638, https://doi.org/10.1080/00405000.2018.1548088.

[28] a. Izzo Renzi, C. Carfagna, P. Persico, Thermoregulated natural leather using phase change materials: an example of bioinspiration, Appl. Therm. Eng. 30 (2010) 1369–1376, https://doi.org/10.1016/j.applthermaleng.2010.02.026.

[29] Bendkowska, Experimental study of the thermoregulating properties of nonwovens treated with microencapsulated PCM, Fibres Text. East. Eur. 17 (2009) 87–91.

[30] H. Yoo, J. Lim, E. Kim, Effects of the number and position of phase-change material-treated fabrics on the thermo-regulating properties of phase-change material garments, Textil. Res. J. 83 (2012) 671–682, https://doi.org/10.1177/0040517512461700.

[31] R. Rossi, W. Bolli, Phase change materials for improvement of heat protection, Adv. Eng. Mater. 7 (2005) 368–373, https://doi.org/10.1002/adem.200500064.

[32] H. Zhang, G. Song, H. Ren, J. Cao, The effects of moisture on the thermal protective performance of firefighter protective clothing under medium intensity radiant exposure, Textil. Res. J. 88 (2018) 847–862, https://doi.org/10.1177/0040517517690620.

[33] J.W.S. Hearle, W.E. Morton, Physical Properties of Textile Fibres, fourth ed., Woodhead Publishing Limited, 2008.

[34] DuPont, Technical Guide for NOMEX Brand Fiber, 2001.

[35] S.F. Neves, J.B.L.M. Campos, T.S. Mayor, On the determination of parameters required for numerical studies of heat and mass transfer through textiles - methodologies and experimental procedures, Int. J. Heat Mass Tran. 81 (2015) 272–282, https://doi.org/10.1016/j.ijheatmasstransfer.2014.09.038.

[36] E. Onofrei, T.C. Codau, S. Petrusic, G. Bedek, D. Dupont, D. Soulat, Analysis of moisture evaporation from underwear designed for fire-fighters, Autex Res. J. 15 (2015) 35–47, https://doi.org/10.2478/aut-2014-0015.

[37] H. Zhang, G. Song, H. Ren, J. Cao, The effects of moisture on the thermal protective performance of firefighter protective clothing under medium intensity radiant exposure, Textil. Res. J. 88 (2018) 847–862, https://doi.org/10.1177/0040517517690620.

[38] D.A. Torvi, Heat Transfer in Thin Fibrous Materials under High Heat Flux Conditions, 1997.

[39] Y. Su, J. Li, X. Zhang, A coupled model for heat and moisture transport simulation in porous materials exposed to thermal radiation, Transport Porous Media 131 (2020) 381–397, https://doi.org/10.1007/s11242-019-01347-2.

[40] Rubitherm PCMs, n.d. http://www.rubitherm.de/english/pages/02a_latent_heat_pcms.htm.

[41] H. Zhang, X. Liu, G. Song, H. Yang, Effects of microencapsulated phase change materials on the thermal behavior of multilayer thermal protective clothing, J. Textil. Inst. (2020) 1–10, https://doi.org/10.1080/00405000.2020.1832363, 0.

[42] M. Salloum, N. Ghaddar, K. Ghali, A new transient bioheat model of the human body and its integration to clothing models, Int. J. Therm. Sci. 46 (2007) 371–384, https://doi.org/10.1016/j.ijthermalsci.2006.06.017.

[43] M.P. Castellani, T.P. Rioux, J.W. Castellani, A.W. Potter, X. Xu, A geometrically accurate 3 dimensional model of human thermoregulation for transient cold and hot environments, Comput. Biol. Med. 138 (2021), https://doi.org/10.1016/j.compbiomed.2021.104892.

[44] M.S. Ferreira, J.I. Yanagihara, A transient three-dimensional heat transfer model of the human body, Int. Commun. Heat Mass Tran. 36 (2009) 718–724, https://doi.org/10.1016/j.icheatmasstransfer.2009.03.010.

[45] F.C. Henriques, Studies of thermal injury V. The predictability and the significance of thermally induced rate processes leading to irreversible epidermal injury, Arch. Pathol. 43 (1947) 489–502.

[46] Y. Su, J. Li, Development of a test device to characterize thermal protective performance of fabrics against hot steam and thermal radiation, Meas. Sci. Technol. 27 (2016), 125904, https://doi.org/10.1088/0957-0233/27/12/125904.

[47] M.K. Donnelly, W.D. Davis, J. Lawson, M. Selepak, Thermal Environment for Electronic Equipment Used by First Responders, vol. 1474, National Institute of Standards and Technology Special Publication, 2006, p. 41.

[48] G.N. Mercer, H.S. Sidhu, A theoretical investigation into phase change clothing benefits for firefighters under extreme conditions, Chem. Prod. Process Model. 4 (2009), https://doi.org/10.2202/1934-2659.1349.

[49] H. Zhang, G. Song, H. Ren, J. Cao, The effects of moisture on the thermal protective performance of firefighter protective clothing under medium intensity radiant exposure, Textil. Res. J. 88 (2018) 847–862, https://doi.org/10.1177/0040517517690620.

[50] A. Fonseca, S.F. Neves, J.B.L.M. Campos, Thermal performance of a PCM firefighting suit considering transient periods of fire exposure, post – fire exposure and resting phases, Appl. Therm. Eng. 182 (2020), 115769, https://doi.org/10.1016/j.applthermaleng.2020.115769.

[51] A. Fonseca, T.S. Mayor, J.B.L.M. Campos, Guidelines for the specification of a PCM layer in firefighting protective clothing ensembles, Appl. Therm. Eng. 133 (2018) 81–96, https://doi.org/10.1016/j.applthermaleng.2018.01.028.

fans, Int. J. Heat Mass Tran. 126 (2018) 636–648, https://doi.org/10.1016/j.ijheatmasstransfer.2018.05.155.